Diverse transcriptome reprogramming trajectories underlie quantitative disease resistance at the species level

Florent Delplace[a]*, Mehdi Khafif[a] and Sylvain Raffaele[a]*

Affiliations :

[a]Laboratoire des Interactions Plantes-Microbes Environnement (LIPME), INRAE, CNRS, Université de Toulouse, 31326 Castanet-Tolosan, France

Corresponding authors :

* Florent Delplace : florent.delplace@inrae.fr

* Sylvain Raffaele : sylvain.raffaele@inrae.fr

Running Title :

Species-wide diversity of responses to *Sclerotinia*

Classification: Biological Sciences, Plant Biology

Keywords: plant-pathogen interactions, immunity, quantitative disease resistance, transcriptome, genes network

Abstract

Quantitative disease resistance (QDR) is an immune response limiting the damage caused by pathogen infection in plants. It involves the transcriptomic reprogramming of numerous genes each having a weak contribution to the plant immunity phenotype. Despite QDR widespread and broad-spectrum nature, the evolution of the underlying transcriptome reprogramming remains largely uncharacterized. Here, we analyzed global gene expression in response to the necrotrophic fungus *Sclerotinia sclerotiorum* in 23 *Arabidopsis thaliana* accessions of diverse origin and contrasted QDR phenotype. Over a half of the species pan-transcriptome displayed local responses to *S. sclerotiorum*, with global reprogramming patterns incongruent with accessions phylogeny. Due to frequent small-amplitude variations, only ~11% responsive genes were common to all accessions. They formed protein-protein interactions networks densely connecting both old and recent genes. Clustering of accessions based on global regulation patterns identified four subsets unrelated to QDR phenotypes, highlighting at least four distinct paths towards regulatory evolution of QDR at the species level. We identified WRKY and MYB-related DNA binding sites enriched in the 5'-regulatory regions of core and subset-specific responsive genes respectively. Our findings show that the evolution of QDR involves distinct gene reprogramming trajectories at the species level, associated with contrasted patterns of cis-regulatory variation.

40 ## Introduction

41 Plants actively respond to pathogens attacks by modulating their physiology, using a
42 range of molecular mechanisms to detect pathogens and defend against them. Gene-for-gene
43 resistance is an immunity mechanism which involves single dominant resistance genes
44 belonging to the nucleotide-binding domain and leucine-rich repeat (NLR) or Receptor Like
45 Protein (RLP) families (Dodds and Rathjen, 2010). Quantitative disease resistance (QDR) is
46 another form of plant immunity that limits the damage caused by pathogen infection which is
47 nearly universal, often durable and broad-spectrum (Roux *et al.*, 2014; Corwin and
48 Kliebenstein, 2017). QDR requires genes from very diverse families, each having a small effect
49 on resistance (Gou *et al.*, 2023), which makes the identification and characterization of QDR
50 genes difficult. Interestingly, QDR is the only form of plant immunity that reduces disease
51 symptoms caused by many organisms that actively kill host cells for infection, such as the
52 necrotrophic pathogen *Sclerotinia sclerotiorum* (Niks *et al.*, 2015; Wang *et al.*, 2019). This
53 devastating pathogen is responsible for white and stem mold diseases on a broad range of
54 dicot plants (Bolton *et al.*, 2006), and notably causes severe damage on Brassicaceae, including
55 *Arabidopsis thaliana*, when conditions are favorable (Derbyshire and Denton-Giles, 2016).

56 A comparison of *Brassica napus* resistant and susceptible lines infected by *S.*
57 *sclerotiorum* revealed 9,001 differentially expressed genes related to pathogen recognition,
58 jasmonic acid/ethylene signaling pathways, WRKY transcription regulation, biosynthesis of
59 defense-related proteins and indole glucosinolates (Wu *et al.*, 2016). Comparative
60 transcriptomics across dicot families identified nearly 10,000 genes mis-regulated by *S.*
61 *sclerotiorum* infection in each species, among which ~40% were genes conserved in the core
62 eudicot clade (Sucher *et al.*, 2020). QDR therefore involves reprogramming of a large number
63 of genes (Pink *et al.*, 2023; Zhang *et al.*, 2019). Their individual contribution to the resistance
64 phenotype is largely unknown but is likely low, in agreement with an infinitesimal model of
65 complex polygenic traits (Nelson *et al.*, 2013; Boyle *et al.*, 2017). Yet, stress-responsive genes
66 and the transcription factors regulating them may play crucial roles in plants adaption to
67 pathogens attacks (Coolen *et al.*, 2016; Shankar *et al.*, 2016; Groen *et al.*, 2020).
68 Understanding how plants adapt their transcriptomes to mitigate damage caused by
69 necrotrophic pathogens is crucial to understand the evolutionary dynamics of complex traits
70 at the transcriptome level, and to document the diversity and functioning of QDR genetic
71 determinants.

72 Upon pathogen attack, plant lineages display diversified metabolic and transcriptomic
73 responses that converge on essential hubs (Han and Tsuda, 2022). The plant immune system
74 likely evolved in a stepwise manner by gradually acquiring various specialized components
75 connected to crucial nodes (Adachi *et al.*, 2019; Pruitt *et al.*, 2021; Iakovidis *et al.*, 2022).
76 Convergent pathways, exemplified by the intricate hormone signaling network, drive the
77 expression of core genes across long evolutionary timescales (Aerts *et al.*, 2021) and buffer
78 metabolic and transcriptomic plasticity of plant defense (Zhang *et al.*, 2017). The evolution of
79 the plant immune system is determined by variation both in coding sequences and in gene
80 expression (Tsuda and Somssich, 2015; Monteiro and Nishimura, 2018). Local diversity in gene
81 expression pattern across species and populations can be responsible for adaptive evolution
82 (Harrison *et al.*, 2012; Lasky *et al.*, 2014). Several studies compared resistant with susceptible
83 plant genotypes (Westrick *et al.*, 2019; Mwape *et al.*, 2021) or used expression Quantitative
84 Trait Loci (eQTL) (Moscou *et al.*, 2011) to point at genomic loci that control gene-expression
85 differences and identify resistance determinants and regulators. However, studies on global
86 expression diversity in response to pathogen at the species level remain scarce, and the extent
87 to which diverse patterns of transcriptome reprogramming can lead to similar QDR phenotype
88 is unclear. Transcriptional differences within species primarily rely on DNA sequence
89 variations, including single nucleotide polymorphisms (SNPs), insertions or deletions (indels),
90 and transposable elements (TEs) (Studer *et al.*, 2011; Ando *et al.*, 2018; Nicole E Soltis *et al.*,
91 2020). Notably, cis-regulatory variations caused by TE-derived enhancers significantly impact
92 abiotic stress response (Ito *et al.*, 2011; Makarevitch *et al.*, 2015) and plant defense (Badet *et*
93 *al.*, 2019; Barco *et al.*, 2019). In addition, variation in transcription factor (TFs) binding motifs
94 in 5'-regulatory regions modulate transcriptomic defense responses, such as in Brassicaceae
95 where the emergence of WRKY TF binding motifs associates with specific response to the
96 bacterial molecular pattern flg22 (Winkelmüller *et al.*, 2021). Cis-regulatory variants, by acting
97 on TFs binding sites, could be a major source of transcriptome adaptation during plant
98 evolution (Filichkin *et al.*, 2011; Yu *et al.*, 2015; Wang *et al.*, 2016), but their contribution to
99 QDR variation at the species level is currently elusive.

100 Despite the widespread nature of QDR and its importance for the durable management
101 of plant diseases, our understanding of QDR evolution is limited to knowledge on specific
102 genes or gene families that were associated to this form of immunity (Badet *et al.*, 2017; Barco
103 *et al.*, 2019). The conservation of global QDR responses at the species level offers a unique

104 opportunity to study the recent evolution of gene expression patterns underlying complex
105 traits such as QDR. In this paper, we explored the intraspecific variation in *A. thaliana*
106 transcriptomic responses to *S. sclerotiorum* across 23 accessions with diverse resistance
107 phenotypes and geographical origins. We combined differential expression,
108 phylostratigraphic, network reconstruction and proximity analyses to reveal four accession
109 subsets with distinct reprogramming patterns. Genes showing the highest association with
110 QDR in each subset were largely non-overlapping. Finally, an analysis of promoter sequences
111 highlighted the recent acquisition of cis-regulatory elements associated with QDR in a subset
112 of *A. thaliana* accessions. These findings advance our understanding of the evolutionary
113 dynamics of immune transcriptome at the species level.
114

115 Materials and Methods:

116 Plant material and RNA sampling

117 *Arabidopsis thaliana* accessions listed in Table S1 were obtained from The Versailles
118 Arabidopsis Stock Center. General information regarding collection location and climate data
119 of these accessions was retrieved from https://1001genomes.org and
120 https://www.worldclim.org. Plants were grown in Jiffy pots under controlled conditions at
121 22°C with a 9-hour light period at an intensity of 120 µmol/m^2/s. Five-week-old plants were
122 inoculated with *S. sclerotiorum* strain 1980 (ATCC18683) on three leaves using 0.5-cm-wide
123 plugs of Potato Dextrose Agar (PDA) medium colonized by the fungus. The agar plugs
124 containing the fungal pathogen were placed on the adaxial surface of leaves, and plants were
125 incubated in trays sealed with plastic wrap to maintain 80% relative humidity. 24 hours after
126 inoculation, leaf rings including the periphery of disease lesions were collected as in (Peyraud
127 *et al.*, 2019). Material obtained from three leaves per plant were pooled as one sample,
128 samples were collected in three to five replicates. Leaves from non-inoculated plants under
129 the same conditions were collected as control at the same time.

130 RNA extraction, sequencing and mapping

131 Samples were ground using glass beads (2.5 mm) and RNA was extracted using NucleoSpin
132 RNA PLUS extraction kits (Macherey-Nagel) following the manufacturer's protocols. The
133 quality of the extracted RNA was assessed using Agilent bioanalyzer nanochips. Libraries

134 preparation and mRNA sequencing was conducted at the GeT-Plage facility (INRAE Castanet
135 Tolosan, France) using the Illumina TrueSeq Stranded mRNA kit, 2x150 base pair reads
136 sequencing with S4 chemistry on a NovaSeq instrument. For each experimental condition
137 (inoculated or non-inoculated), three to five independent biological samples were processed,
138 and their respective Illumina paired-end reads were obtained. These reads were
139 simultaneously aligned to the Arabidopsis Columbia-0 reference genome Araport11, and the
140 *S. sclerotiorum* strain 1980 version 2 genome (Derbyshire *et al.*, 2017), using the pipeline nf-
141 core/rnaseq version 3.12.0 described in https://doi.org/10.5281/zenodo.1400710.

142 **Identification and analysis of Differentially Expressed Genes**

143 Normalization of read counts per gene was performed using the edgeR package considering
144 total read count by library (Robinson *et al.*, 2010). Differential expression analysis was
145 conducted using edgeR package v 3.32.1 in R 4.0.4. using mock treated plants as a reference
146 for each accession with ~replicates + treatment as the design formula. Genes with |Log2 Fold
147 Change (LFC)|≥ 2 and a Benjamini–Hochberg adjusted P-value (FDR) < 0.05 were considered
148 significant for differential expression. Raw and processed gene expression data was deposited
149 in NCBI's GEO under accession number GSE248079. Heatmaps were generated using the
150 heatmap.2 package in R 4.2.1. Hierarchical clustering was performed using the default
151 parameters of hclust, and the robustness of the branches was evaluated with pvclust v2.2-0.
152 Gene Ontology enrichment analysis was performed using BINGO module 3.0.3 from Cytoscape
153 3.9.1, assessing over-representation of GO terms in our gene lists compared all GO terms from
154 *A. thaliana*.

155 Log regression analyses to extrapolate the number of responsive and core genes were done
156 using 'drc' package v3.0-1 in R, the log-logistic (LL.4) model was employed to characterize the
157 relationship between the number of DEGs ('n_genes') and categorical grouping factors
158 ('n_accessions'). The maximal gene expression level was estimated at 10^{12} for 'n_accessions.'.
159 Visualizations were created using the 'ggplot2' package, showcasing boxplots and overlaid red
160 curves representing the fitted exponential trends.

161 Pearson correlation matrix to correlate transcriptomes across accessions, was performed
162 using cor function excluding auto-comparisons from stats package v4.3.1, considering the log
163 fold change (LFC) for all expressed genes. The resulting matrix was subjected to hierarchical

164 clustering using the pheatmap library v1.0.12 in R, with a specified number of clusters (k=4)
165 and the "ward.D" method. The same clustering pattern was obtained using a distance matrix
166 with dist function from stats package v4.3.1.

167 **Phenotypic Characterization of Arabidopsis Accessions in response to *S. sclerotiorum***

168 0.5-cm-wide plugs of PDA agar medium containing *S. sclerotiorum* strain 1980 grown for 72
169 hours at 20°C on 14 cm Petri dishes were placed on the adaxial surface of detached leaves.
170 These leaves were positioned in Navautron system (Barbacci *et al.*, 2020), records were done
171 using high-definition (HD) cameras "3MP M12 HD 2.8-12mm 1/2.5 IR 1:1.4 CCTV Lens". In total
172 33 to 135 leaves from 3 experiments were inoculated per accession. Kinetics of *S. sclerotiorum*
173 disease lesions were analyzed using INFEST script v1.0 (https://github.com/A02l01/INFEST).
174 Statistical analyses of disease phenotypes were conducted using Tukey test in R 4.2.1 as
175 described in (Barbacci *et al.*, 2020).

176 **Phylogenetics tree construction**

177 Phylogenetic trees of the accessions were constructed from all coding sequences (CDS)
178 recovered from the 23 corresponding pseudo-genomes available at the 1001 Genome Project
179 Data Center. For this, pseudo-genomes were annotated using *A. thaliana* functional
180 annotations (TAIR version 10) with liftoff (v1.6.1) (Shumate and Salzberg, 2021). Annotations
181 were converted to coding sequences and protein sequences with gffread (Pertea and Pertea,
182 2020). 21,787 orthology groups were inferred with Orthofinder version 2.5.4 (Emms and Kelly,
183 2019). Orthogroups with a unique copy in each accession were aligned with Mafft (v7.313)
184 (Nakamura *et al.*, 2018). A super alignment was built from the orthogroup alignment by
185 Orthofinder. Accession trees were inferred with IQ-TREE (v2.5.4) (Nguyen *et al.*, 2015). The
186 best models according to the Bayesian Information Criterion (BIC) computed by ModelFinder
187 (Kalyaanamoorthy *et al.*, 2017) were VT+F+I+G4 and GTR+F+I+G4 for the accession tree
188 computed from protein alignments and from coding sequence alignments respectively.
189 Branch support values were computed by two different methods: SH-aLRT (Guindon *et al.*,
190 2010) and UFBoot (Hoang *et al.*, 2018). Accession clustering was done using the cophenetic
191 function from the R package ape v5.7.1. The tanglegram in Figure 1C was generated using
192 phylogenetic tree data and the DEGs heatmap accession dendrogram using cophylo function
193 from phytools v2.1-1.

194 **Orthologs identification and relative gene age estimation**

195 Arabidopsis orthologous gene groups were retrieved using the Phytozome v13 database
196 (Goodstein *et al.*, 2012). These orthogroups were used to assign relative gene age (*Arabidopsis*
197 *thaliana* node to Viridiplantae node) as the species tree node to which the MRCA of species
198 represented in the orthogroup mapped. Enrichment of gene sets in gene age categories were
199 analyzed with Chi-square tests at a significance threshold P-value < 0.05.

200 **Protein-protein network construction**

201 Interactors of the 1.049 upregulated core DEGs among the 23 accessions were retrieved from
202 the Arabidopsis BioGRID protein interaction datasets version 4.4.211 (Oughtred *et al.*, 2021).
203 Protein–protein interactions were visualized and analyzed with Cytoscape software version
204 3.9.1.

205 **Regression analysis, disease score correlation with expression for each gene**

206 To identify genes whose expression correlate with disease phenotype within accession
207 subsets, the mean disease index by accession (hereafter 'slope') was fitted with log fold
208 change (LFC) of expression for each gene (hereafter 'LFC') in corresponding accessions by
209 linear regression. We employed R2 and RMSE as evaluation metrics. R2 quantifies the
210 proportion of variation in dependent variables that can be accounted for by the predictors,
211 while RMSE represents the model's average error. R2 and RMSE were calculated in R using
212 ggplot2 v3.4.2 with the following formulas: R2 = (cor(slope, LFC))^2, and rmse = sum((slope -
213 cov(slope, LFC) / var(LFC) * LogFC - mean(slope) - cov(slope, LFC) / var(LFC) * mean(LFC))^2),
214 a rmse threshold of 0.01 was used. The Top500 QDR-associated genes by subsets were
215 selected based on the highest R2 value and RMSE < 0.01.

216 **Promoter sequence analyses**

217 1Kb promoter sequences were retrieved from https://tools.1001genomes.org/api/ v1b for 22
218 out of 23 accessions (Mt-0 promoter sequences were unavailable). To conduct DNA motif
219 enrichment analysis, we employed MEME Suite 5.5.4 (Bailey *et al.*, 2015) with the Simple
220 Enrichment Analysis (SEA) tool, using the Arabidopsis DAP (DNA Affinity Purification) motifs
221 database from (O'Malley *et al.*, 2016). Enrichment of motifs in promoters of selected gene

222 sets were assessed with Fisher's exact test using the fisher.test function from the R stats
223 package version 3.6.2 within the R environment version 4.0.4.

224 Results

225 *A. thaliana* species pan-transcriptome shows broad but weak variability across individuals

226 To document *A. thaliana* species pan-transcriptome during infection by *S. sclerotiorum*, we
227 performed RNA-sequencing on 23 natural accessions covering a broad range of the species
228 genetic and geographic diversity (Figure 1A). To assess global gene expression profile during
229 infection, total mRNA of healthy leaves and leaves colonized by *S. sclerotiorum* were collected
230 24 hours post-inoculation (hpi) and sequenced. Each sample was collected in independent
231 triplicates to allow the detection of accession-specific differentially expressed genes (DEGs).
232 We obtained an average 32,908,875 reads per sample, 99% of which could be mapped to
233 Araport11 reference transcripts in healthy leaves and 43% in infected leaves (Table S2). A
234 consistent 60.92% ± 1.72% of complete transcriptomes was expressed across the 23
235 accessions in healthy plants, and 54.71% ± 3.51% in infected plants. To identify *S.*
236 *sclerotiorum*-responsive transcripts, we determined DEGs in infected versus healthy leaves for
237 each accession (Figure 1B). The number of DEGs ranged from 6,712 to 9,269, with a majority
238 of DEGs downregulated in every accession (upregulated/downregulated ratio of 0.72 ± 0.11,
239 Table S3-4). DEGs represented an average 39.56% ± 2.80% of expressed genes in each
240 accession. Overall, 17,340 genes corresponding to 52.36% of *A. thaliana* transcriptome were
241 differentially expressed in at least in one accession. Phylogenetic tree based on CDS derived
242 from pseudogenomes defined five genetic groups that correspond to geographical or climate
243 proximity (Figure 1A, 1C). Comparison between phylogenetic tree of accessions and gene
244 expression dendrogram did not show clear congruence (Figure 1C). To estimate the size of *S.*
245 *sclerotiorum*-responsive transcriptome at the species level, we performed random accession
246 sampling and logarithmic regression fit. This predicted a maximum of 22,643 DEGs (68.4% of
247 the predicted transcriptome) across the whole *A. thaliana* diversity with R^2=0.947 (Figure 1D).
248 Among DEGs, 51.5% showed a maximum distance of LFC < 2 between accessions, and 2.6 %
249 had a maximum distance of LFC > 10 (Figure S1), indicating that drastic changes of expression
250 profiles across accessions are limited to a few genes.

These results show that *S. sclerotiorum* infection triggers reprogramming of a majority of *A. thaliana* species pan-transcriptome, with weak variations across accessions and a generally weak phylogenetic signal.

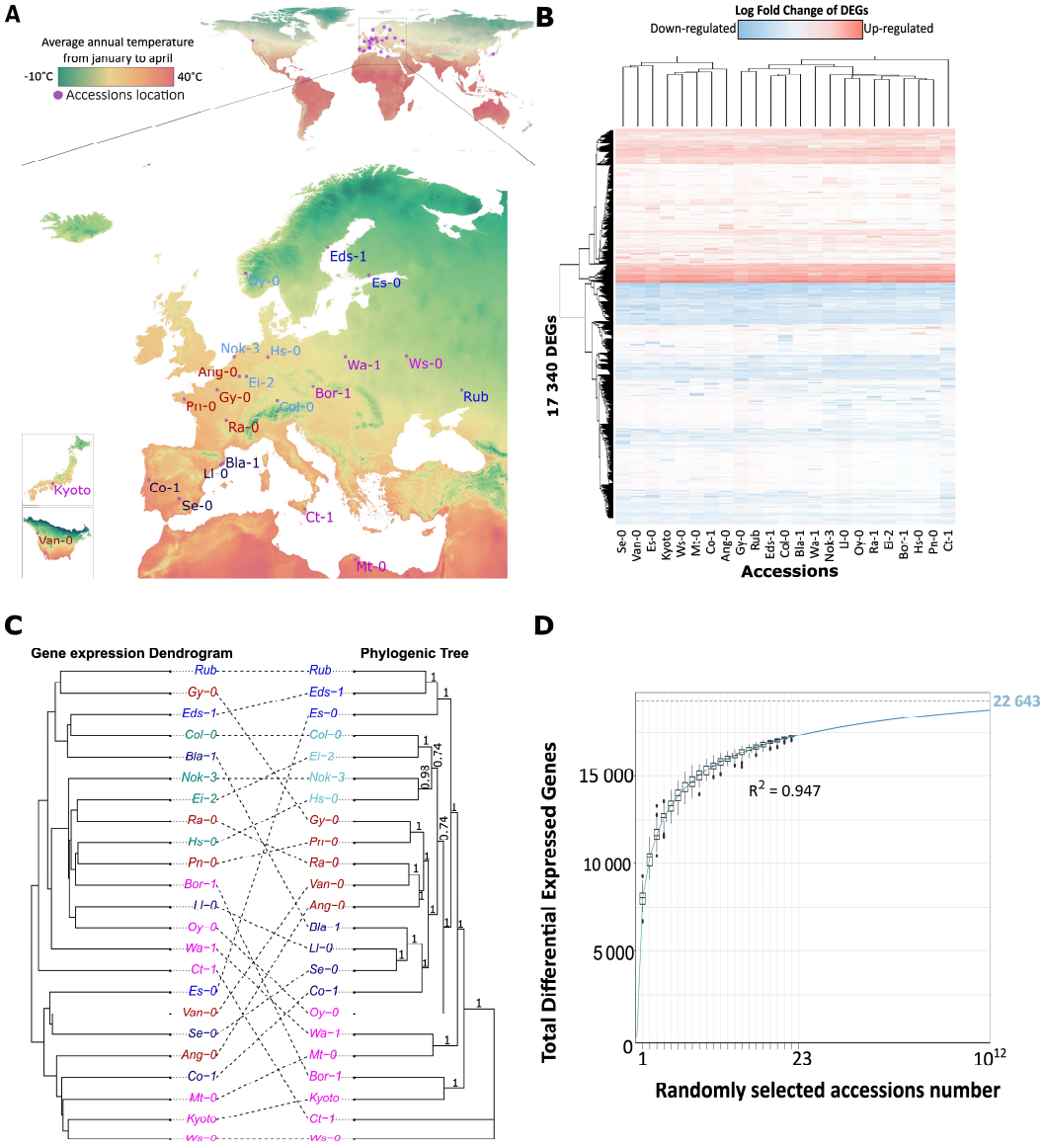

Figure 1: The 23 accessions exhibit similar expression profiles during Sclerotinia infection, unrelated to phylogeny.

A. Distribution of the 23 accessions across Europe, Canada, and Japan. Purple dots represent the coordinates of the initial collection locations for each accession. The background color indicates the mean spring temperature, with blue indicating the coldest regions and red indicating the warmest. The five accessions color groups represent five genetic groups defined in phylogenic tree in Figure 1C. **B**. Heatmap displaying the distribution of 17.340 significantly differentially expressed genes (DEGs) in the 23 accessions after Sclerotinia infection, with $|LFC| \geq 2$. **C**. Tanglegram comparing the gene expression dendrogram in Figure 1B to the phylogenetic tree based on coding sequences (CDS) across the 23 accessions. The label colors indicate the five main phylogenetic clusters, and the numbers at the branches represent confidence values obtained using the UFBoot2 bootstrap method. **D**. Exponential regression analysis estimating the maximum number of DEGs through random sampling from 1 to 23 accessions. The regression curve, with an R^2 coefficient of 0.947, suggests a maximum of 22,643 DEGs with 10^{12} accessions.

268 **About 11% of *S. sclerotiorum* responsive genes are differential in all *A. thaliana* accessions**

269 To determine transcriptional responses to *S. sclerotiorum* conserved at the species level, we
270 compared the expression profile of the 17,340 DEGs across 23 accessions (Figure 2A). DEGs
271 with a differential expression in one accession only (accessory) ranged from 36 to 292, making
272 a total 2,202 accessory DEGs (12.7%) at the species level. There were 13,181 DEGs (76%)
273 differential in two to 22 accessions (shell). We identified 1,957 DEGs (11.3%) differential in all
274 accessions (core) including 1,049 upregulated core DEGs and 908 downregulated core DEGs.
275 Among the 17,340 DEGs, 1221 (7.0%) showed opposite regulation patterns (up- versus down-
276 regulated) in at least two accessions. The number of DEGs with opposite regulation decreased
277 from 13% for DEGs differential in two accessions to 0% in core DEGs (Figure 2A, B). Core DEGs
278 were consistently up- or down-regulated in all 23 accessions and showed a high expression
279 stability (Figure 2B, Figure S2). Up/down regulated DEGs ratio was 1.16 in core DEGs, 0.76 in
280 accessory DEGs and 0.60 in shell DEGs, suggesting an accumulation of genes upregulated upon
281 *S. sclerotiorum* inoculation during *A. thaliana* evolution.

282 Using regression analysis, we estimated a minimum core DEG set of 719 upregulated and 352
283 down regulated genes across the whole *A. thaliana* diversity (Figure 2C-D). Therefore, out of
284 22,643 genes predicted responsive to *S. sclerotiorum* at the species level (Figure 1D), only
285 1,071 (4.7%) are predicted core DEGs. Our analysis based on 23 accessions likely
286 overestimated the species-level core DEG sets but identified core up-regulated and core
287 down-regulated genes from DEGs. To determine the functional landscape of core DEGs, we
288 performed a Gene Ontology (GO) enrichment analyses. GOs corresponding to 254 Biological
289 Processes were significantly enriched among the upregulated core DEGs (Figure 2C). Majority
290 of these GOs corresponded to ontologies related to primary metabolism, secondary
291 metabolism, molecules transport and defense responses. Precisely, GOs related to secondary
292 metabolism included camalexin biosynthetic process (GO:0010120), chorismate metabolic
293 process (GO:0046417) and lignin biosynthetic process (GO:0009809), GOs related to defense
294 responses included pattern recognition receptor signaling pathway (GO:0002221), response
295 to ethylene (GO:0009723) and jasmonic acid mediated signaling pathway (GO:0009867). Core
296 Up DEGs included defense related genes such as *ABCG30*, *CERK1*, *PAD3*, *RBOHD* and *RLP30*
297 (Stotz *et al.*, 2011; Zhang *et al.*, 2013; Zhou *et al.*, 2013; Sucher *et al.*, 2020; Pi *et al.*, 2023).
298 GOs corresponding to 154 Biological Processes were significantly enriched among the down

regulated core DEGs (Figure 2D), including responses to light, developmental responses or photosynthesis.

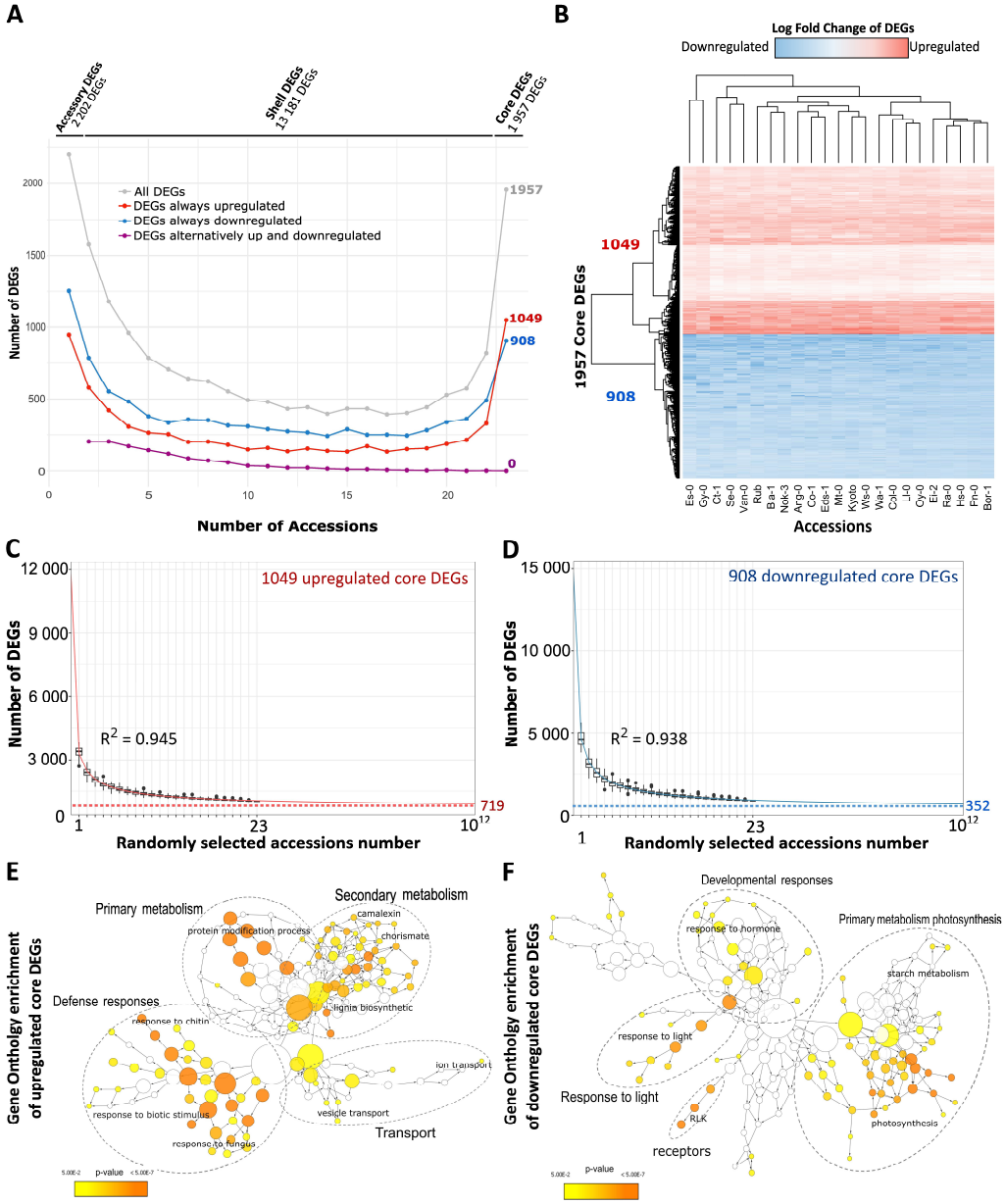

Figure 2. 1.957 core DEGs are differentially expressed across the 23 accessions.
A. Number of genes differentially expressed in 1 to 23 accessions. Grey dots represent all DEGs deregulated in 1 to 23 accessions, while red and blue dots indicate DEGs that are upregulated or downregulated in the considered accessions, respectively. Purple dots highlight DEGs present in at least one upregulated and one downregulated state across the considered accessions. **B.** Heatmap displaying the distribution of 1.957 core differentially expressed genes (DEGs) across the 23 accessions after *Sclerotinia* infection, with an absolute log-fold change (|LFC|) ≥ 2. Red panels correspond to 1.049 genes significantly upregulated, and blue panels correspond to 908 downregulated genes. **C and D.** Exponential regression analysis estimating the minimal number of core upregulated (C) or downregulated (D) DEGs through random sampling from 1 to 23 accessions. The regression curves, with a regression coefficient of R^2= 0.945 and R^2= 0.938 respectively, suggest a minimum of 719 core upregulated DEGs and 352 core downregulated DEGs as the number of accessions is 10^{12}. **E and F**. Gene Ontology (GO) enrichment analysis of the 1.049 core upregulated DEGs (E) and the 908 core downregulated DEGs (F), plotted using the BINGO module from the Cytoscape software. Enrichment was calculated using BINGO and visualized on the GO hierarchy using Cytoscape. Circle size represents the number of genes in one GO category.

316 **Network connectivity of upregulated core DEGs is not related to gene age**

317 To study the evolutionary dynamics of core DEGs, we performed a phylostratigraphic analysis
318 using Phytozome orthogroups. 1,039 upregulated core DEGs and 899 downregulated core
319 DEGs were included in Phytozome orthogroups. Core *S. sclerotiorum*-responsive genes
320 showed a clear gene age pattern with dominant old genes (Viridiplantae and Embryophyta)
321 and young genes (Brassicaceae and *A. thaliana*) to a lesser extent, creating skewed U-shaped
322 distributions (Figure 3A). These distributions are similar to those of all *A.thaliana* genes,
323 indicating that *A. thaliana* transcriptome is dominated by old and young genes. Compared to
324 all *A. thaliana* genes, core DEGs included significantly fewer young genes and more old genes
325 (+17.6% for upregulated core DEGs, +21.6% for downregulated core DEGs). Relative to *A.*
326 *thaliana* whole genome, accessory DEGs included fewer old genes (-1.7%) while shell DEGs
327 were enriched in old genes (+ 4.2%). These patterns suggest that intra-specific expression
328 variation is better tolerated in young genes.

329 To test whether the age of core DEGs related to network connectivity, we constructed the
330 protein–protein interaction (PPI) network of upregulated core DEGs based on the BioGrid
331 database. This network included proteins encoded by 351 core upregulated DEGs (29%), 2,474
332 other proteins and 9,870 PPIs (Figure 3A). The mean topological coefficient was 0.196 for all
333 351 core upregulated DEGs, 0.187 for Viridiplantae core DEGs and 0.234 for Brassicaceae core
334 DEGs (23 genes, Figure 3C). Other Brassicaceae and Viridiplantae proteins of the network had
335 a mean topological coefficient of 0.194, suggesting that despite a late appearance in evolution,
336 Brassicaceae core DEGs quickly acquired a central place in protein networks. We identified
337 239 interactions between Brassicaceae core DEGs and Viridiplantae proteins (average 8.9
338 interactions per Brassicacea core DEGs, 12.6 for Viridiplantae core DEGs) and 149 interactions
339 with Embryophyta proteins (Figure 3D). High protein connectivity may therefore act as a
340 selective force rapidly stabilizing pathogen responsiveness at the species level. Brassicaceae
341 core upregulated DEGs included some well-known immune genes such as *AIG2*, *BIK1*,
342 *EXO70B2*, *LECRK*, *PAD3*, *PROPEP1* and *SYP122* (Eckardt, 2011; Stotz *et al.*, 2011; Desclos-
343 Theveniau *et al.*, 2012; Brillada *et al.*, 2021; Rubiato *et al.*, 2022; Zhang *et al.*, 2022; Wang *et*
344 *al.*, 2022) suggesting that differential expression of these genes could contribute to resistance
345 against *S. sclerotiorum*.

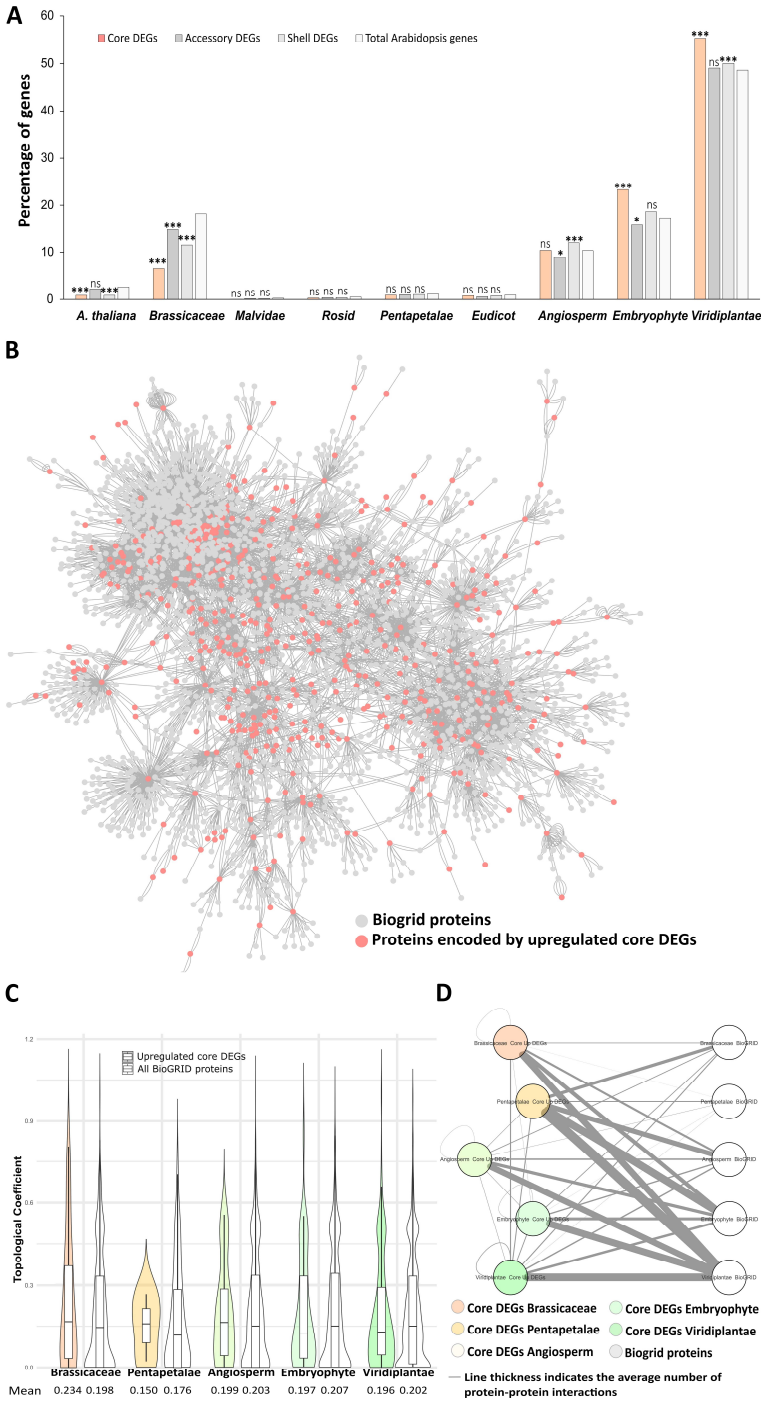

Figure 3: Overview of upregulated core DEGs conservation and their place within a protein-protein interaction network.

A. Conservation of core DEGs during extended evolutionary periods. Ancestral characteristics of DEGs were retrieved from the Phytozome database. Orange corresponds to core DEGs (upregulated and downregulated), grey to accessory DEGs, light grey to shell DEGs and white to the total genes in the Arabidopsis Phytozome database. **B.** The protein-protein interaction network, plotted using Cytoscape, displays the components used for its construction: in orange, the proteins encoded by core upregulated DEGs, and in gray, the proteins identified in the bibliography as experimentally interacting with the proteins corresponding to the proteins encoded by core upregulated DEGs. **C.** Topological coefficients associated to core upregulated Brassicaceae, Pentapetalae, Angiosperm, Embryophyte or Viridplaatae DEGs encoded proteins present in protein-protein

interaction network. White violin plot corresponds to the Topological coefficients associated with Brassicaceae, Pentapetalae, Angiosperm, Embryophyte, or Viridiplantae from all BioGRID database proteins. **D**. Average number of protein-protein interaction numbers between core upregulated Brassicaceae, Pentapetalae, Angiosperm, Embryophyte or Viridplantae DEGs encoded proteins and Brassicaceae, Pentapetalae, Angiosperm, Embryophyte or Viridplantae BioGrid proteins. Protein-protein interactions between BioGRID proteins were not used during core upregulated DEGs centralized network construction. Size grey connecting bars are proportional to average protein-protein interaction.

Disease resistance associates with quantitative expression variation specific to accession subsets

To relate gene expression with disease resistance variation at the species level, we first evaluated the speed of necrotic lesions progression over time (expressed as the slope of lesion size as a factor of time) (Barbacci *et al.*, 2020) following the inoculation of detached leaves of 23 accessions by *S. sclerotiorum* (Figure 4A). Susceptibility ranged from slope 0.0226 (Se-0) to 0.0667 (Co-1) representing a ~3 fold increase in susceptibility. In order to associate accession susceptibility and transcriptome responses during *S. sclerotiorum* infection, we used expression log fold change (LFC) for all expressed genes to correlate transcriptomes across accessions. Pearson correlation was calculate between each transcriptome to assess the overall proximity between accessions. Based on similarity of global gene expression patterns we identified 4 subsets of 7, 6, 5 and 5 accessions largely consistent with the DEG-based dendrogram from figure 1C (Figure 4B). The obtained clustering pattern was consistent with those obtained through distance matrix analyses. We found no evidence for a link between correlation matrix clustering and environmental parameters at the geographic origin of the accessions (Table S5). We found also no significant correlations between transcriptome subsets and phylogenetic clusters, indicating the absence of a phylogenetic signal to define the four subsets. Each subset included accessions of contrasted resistance levels indicating that QDR variation associates with at least four distinct patterns of global gene reprogramming upon inoculation at the species level.

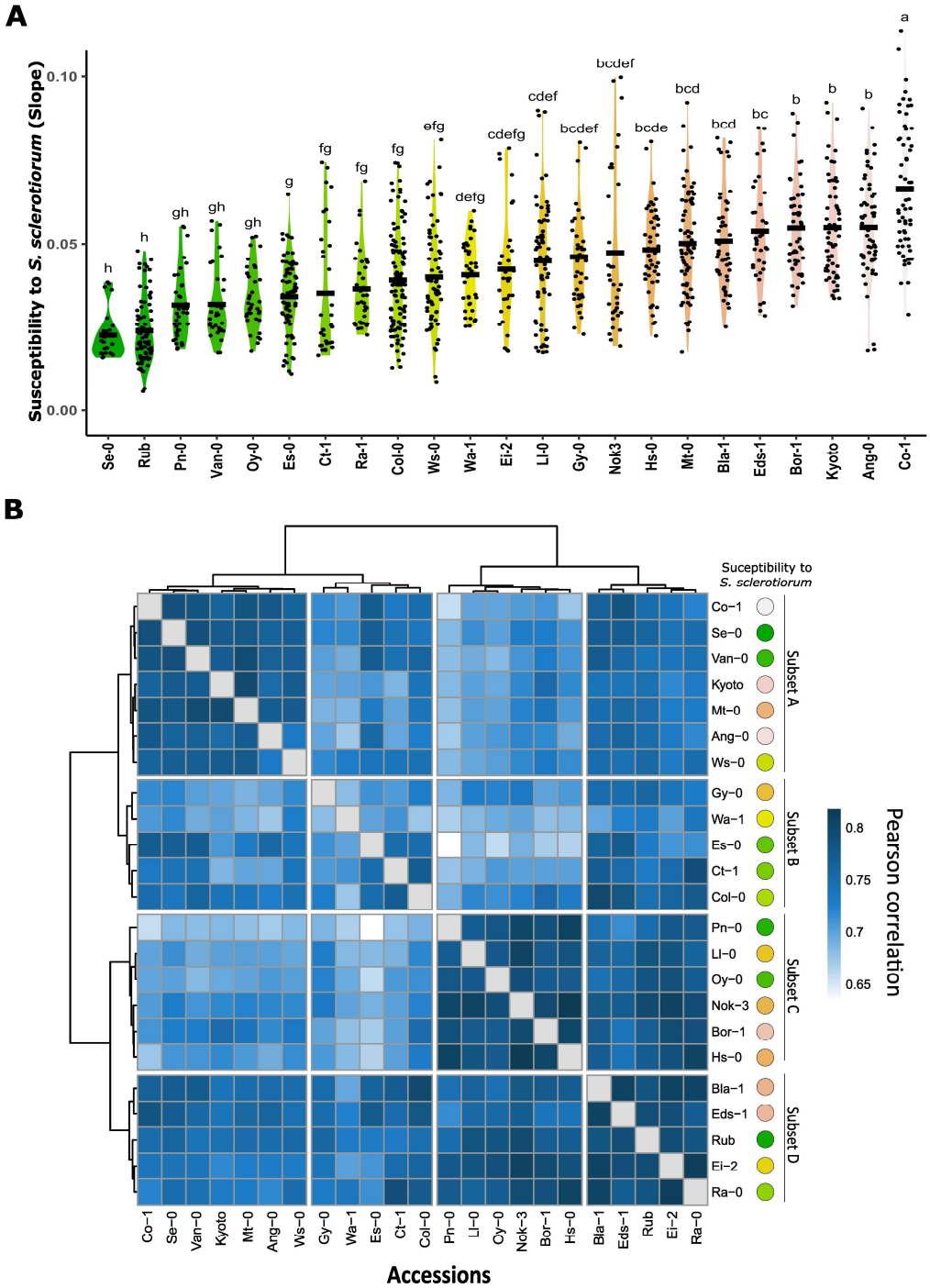

Figure 4: Global gene expression similarity in response to *S. sclerotiorum* reveals 4 accession subsets

A. Susceptibility of 23 accessions at 24 hours after inoculation with a 0.5cm plug on detached leaves. The logarithm of the slope (infection speed) was measured for 33 to 135 leaves in three experiments, with the black horizontal bar representing the mean slope. The color gradient from green to red indicates the range from the most resistant accessions to the most susceptible to Sclerotinia infection. Letters represent statistically grouped results obtained with the Tukey test. **B.** Pearson correlation matrix of the 23 accessions based on global transcriptome profiles during infection. Accession subsets A, B, C, and D are highlighted. Color circles indicates susceptibility to *S. sclerotiorum* for the 23 accessions according to Figure 4A.

394 **Presence-absence of DAP promoter motifs associates with transcriptional response to *S.***
395 ***sclerotiorum***

396 To document the genetic basis for expression variation upon *S. sclerotiorum* inoculation in *A.*
397 *thaliana* accession subsets, we determined the correlation between QDR and the expression
398 levels of all genes in each of the four accession subsets using a regression analysis. We
399 identified the top 500 genes with the highest $|R^2|$ with QDR within each subset (Figure 5).
400 Within accession subsets, 43% ± 13% genes exhibited positive correlation with resistance
401 against *S. sclerotiorum*. Comparison of the four top500 lists revealed that 92% were uniquely
402 correlated to QDR in a single accession subset (top500^{A} to top500^{D}, Figure 5B). This approach
403 did not identify genes associated with QDR in all accession subsets, indicating distinct
404 recruitment of resistance or susceptibility genes in each subset. Among top500^{A-D} genes, 8.2%
405 corresponded to core DEGs, 72.2% to shell DEGs, and 5.2% to accessory DEGs as defined in
406 Figure 2. To further support the specificity of QDR association in each accession subset, we
407 analyzed QDR-expression correlation values for each top500 gene lists in each accession
408 subsets (Figure 5C). 91.9% of top500^{A-D} genes showed highest correlation in their respective
409 accession subset, supporting the view that expression of these genes explained resistance
410 variation specifically within their respective accession subsets.

411 To provide evidence that cis-regulatory variation contributes to expression polymorphism in
412 QDR-related genes at the species level, we tested for DNA affinity purification (DAP) motif
413 enrichment in promoter regions across 22 accessions. First, considering the top500^{A} genes,
414 we identified 236 DAP motifs significantly enriched in the promoter of alleles from subset A
415 accessions compared to orthologs from subsets B, C, and D accessions. We highlight 15 DAP
416 motifs explaining LFC variations among top500^{A} alleles (Fisher's exact test p-val<0.01) present
417 in 364 (34.58%) to 31 (0.58%) promoter sequences (Figure 5E). Among those, the
418 MYBrelated_tnt,AT5G56840_colamp_a_m1 motif bound by the transcription factor
419 AT5G56840 was detected in the promoter of 227 out of 500 genes, in 1 to 6 accessions from
420 subset A (Figure S3). To support a role for the MYBrelated_tnt,AT5G56840_colamp_a_m1 DAP
421 motif in the regulation of top500^{A} alleles, we compared the distribution of LFC upon *S.*
422 *sclerotiorum* infection in top500^{A} alleles harboring or not this motif in their promoter. We
423 found a significant decreased in LFC (by 0.81 in average) for genes harboring the
424 MYBrelated_tnt,AT5G56840_colamp_a_m1 DAP motif compared to control genes (Figure 5E).

425 Second, we searched for DAP motifs enriched in upregulated core DEGs relative to top500^{A-D}
426 genes. This identified 34 WRKY DAP motifs enriched in upregulated core DEGs, present in up
427 to 90.85% (WRKY29_colamp_a DAP motif) in their promoter sequences (Figure F, Table S6).
428 Upregulated core DEGs harboring a WRKY29 DAP motif present a significant average increased
429 of 1.31 in LFC compared to upregulated top500^{ABCD} genes (Figure 5G).

430 This revealed differential acquisition of DAP motifs in cis-regulatory regions of core
431 upregulated DEGs and QDR-associated alleles in subset of *A. thaliana* accessions, possibly
432 reflecting ancestral and more recent acquisitions respectively. Our study highlights the
433 significant impact of presence-absence polymorphism at cis-regulatory DAP motifs on gene
434 responsiveness to *S. sclerotiorum* infection at the *A. thaliana* species level.

435

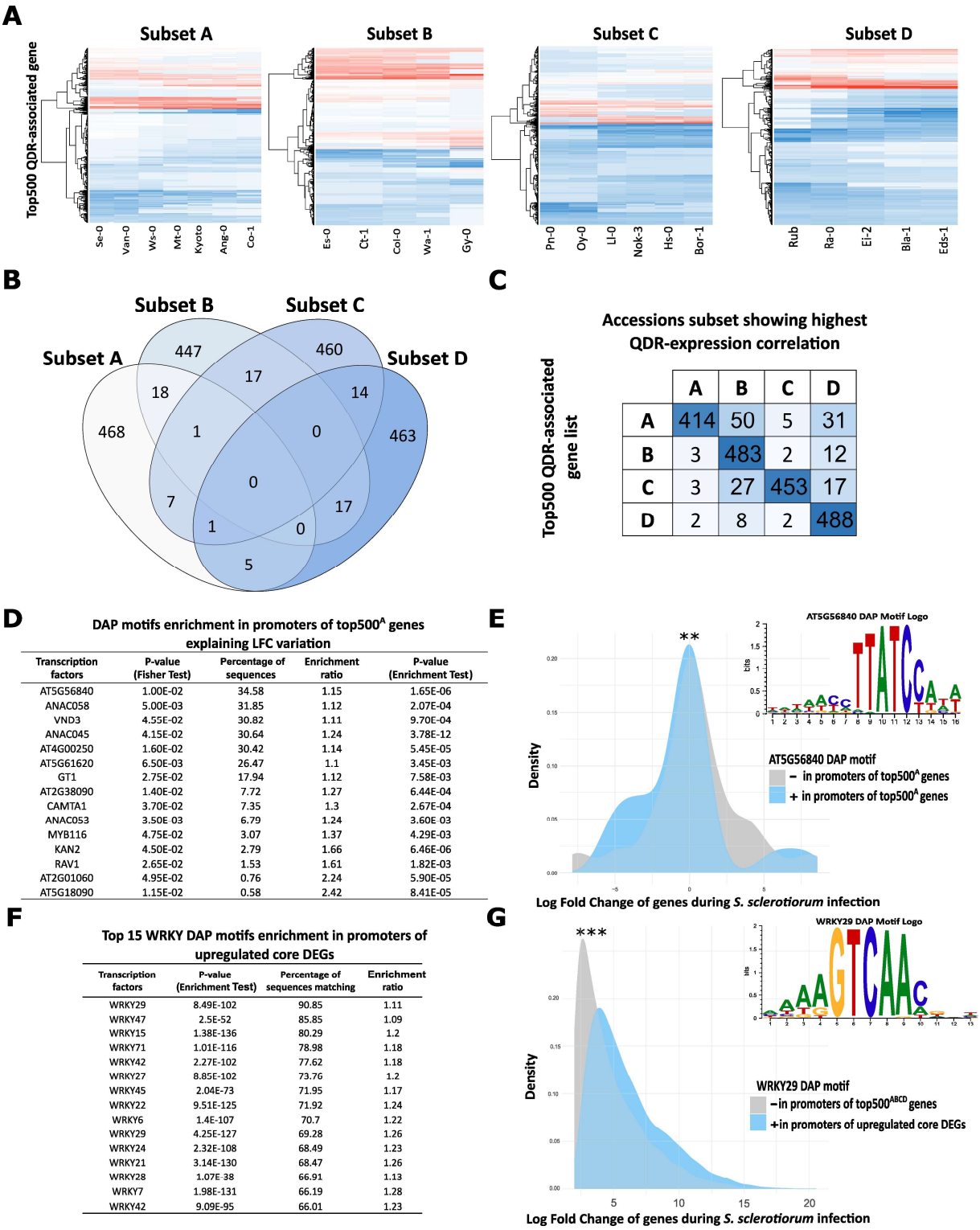

Figure 5. Exploring genes expression variation explaining resistance variation across accessions subsets.

A. Heatmap showing expression profiles of the top 500 QDR-mediated genes across the four corresponding accessions subsets. Red corresponds to up-regulated genes, and blue corresponds to down-regulated genes. **B.** Venn diagram comparing the top 500 QDR-associated gene lists corresponding to the four accessions subsets. **C.** Number of genes from the top 500 QDR-associated genes placed in their association cluster showing the highest QDR-expression correlation. **D**. Table of

444 DAP motifs significantly enriched in promoters of top500^{A} genes compared to the promoters of the
445 top 500^{BCD} genes, which significantly affect gene expression within the A subset of accessions. **E.** The
446 most frequent AT5G56840_colamp_a_m1 DAP motif explaining gene expression modulation in
447 accessions subset A. Differential gene expression for genes showing a presence or absence of
448 AT5G56840_colamp_a_m1 DAP motif in promoter sequences across accessions subset A. ** indicate
449 p-value = 1.65e-06 from fisher test. **F**. Table of top15 WRKY29 DAP motifs significantly enriched in
450 promoter of upregulated core DEGs compared in promoters of the top 500^{ABCD} genes. **G.** The most
451 frequent WRKY DAP motif, WRKY29_colamp_a, significantly enriched in promoters of upregulated core
452 DEGs compared to promoters of top500^{ABCD} genes. Differential gene expression for genes with a LFC
453 >2 with WRKY29_colamp_a DAP motif in promoters of upregulated core DEGs or without
454 WRKY29_colamp_a DAP motif in promoter of top500^{ABCD} genes. *** indicate p-value = 2.2e-16 from
455 Wilcoxon test.

456

457 # Discussion:

458

459 Quantitative disease resistance provides partial and durable protection against various pathogenic
460 species across the green lineage. Genetic mechanisms associated with the short and long-term
461 evolution of QDR remain largely obscure (Kou and Wang, 2010). In a previous study, comparative
462 transcriptome analysis across plant species highlighted exaptation through regulatory divergence as a
463 path towards the evolution of QDR against *S. sclerotiorum* (Sucher *et al.*, 2020). Here we analyzed
464 patterns of QDR transcriptome evolution at the species level through a comprehensive RNAseq
465 analysis of 23 *Arabidopsis thaliana* accessions displaying varying degrees of resistance to *S.*
466 *sclerotiorum* .

467

468 **How complex is plant quantitative disease resistance?**

469 The omnigenic model of complex traits proposes that most genes expressed in an infection context
470 should contribute to the heritability of disease resistance, either through a role in immunity or in its
471 regulation (Boyle *et al.*, 2017). Interspecific comparison found an average 32.63% genes responsive to
472 *S. sclerotiorum* across Pentapetalae, an estimate resulting from the analysis of a single genotype of
473 each species (Sucher *et al.*, 2020). Here we assessed infra-specific variation in *Arabidopsis thaliana*
474 gene responsiveness to *S. sclerotiorum*. In each accession, DEGs represented an average 39. 6% of
475 expressed genes, together accounting for 52.4% of *A. thaliana* pan-transcriptome responsive to *S.*
476 *sclerotiorum* infection. This number is consistent for instance with 50.4% of *A. thaliana* genes
477 differentially regulated upon *Fusarium oxysporum* inoculation (Guo *et al.*, 2021) and suggests that
478 infra-specific variation may expand the repertoire of QDR genes by ~1.3 fold. We have chosen to map
479 RNA-seq reads to the TAIR10 reference genome for a more accurate quantification of gene expression.
480 This approach does not allow to identify accession-specific transcripts that are absent from the

481 reference genome, and probably underestimates slightly the overall diversity of *S. sclerotiorum*
482 responsive transcripts in *A. thaliana*.

483 Among *S. sclerotiorum*-responsive genes in *A. thaliana*, we identified 1049 core up-regulated in all
484 accessions, suggesting either a role in mediating resistance across various genetic backgrounds (Sucher
485 *et al.*, 2020; D., Yang *et al.*, 2021) or broad-spectrum manipulation by the fungus. Gene Onthology
486 analysis associated core upregulated DEGs with general responses to fungal pathogens, such as the
487 biosynthesis of camalexin, chorismate metabolism, and lignin biosynthesis (Zhu *et al.*, 2013; Zhang *et*
488 *al.*, 2017). These processes, conserved at the species level, typically contribute to a broad-spectrum
489 defense against fungal pathogens, including *Botrytis cinerea*, *Colletotrichum higginsianum*, and
490 *Phytophthora parasitica* (Le Berre *et al.*, 2017; Nicole E. Soltis *et al.*, 2020; Zhu *et al.*, 2023). Core DEGs
491 form a bottleneck network where fine-tunable transcriptome modules play a pivotal role in responding
492 to pathogen genetic diversity (Kim *et al.*, 2014; Hillmer *et al.*, 2017). Mutants in the core DEGs *pad3-1*,
493 *abcg40-2* and *rlp30-1* show increased susceptibility to *S. sclerotiorum*, indicating clear contribution of
494 some core DEGs to QDR (Zhang *et al.*, 2013; Sucher *et al.*, 2020; Kusch *et al.*, 2022). However, the
495 relative contribution of many core DEGs to disease resistance remains to be tested, and why the global
496 pool of core DEGs contributes to different levels of resistance across accessions is unclear. The
497 contribution of core genes to QDR may be regulated at the post-transcriptional level in a contrasted
498 manner across accessions. Alternatively, specific core transcript ratio may be required for efficient
499 QDR, or the precise timing of core transcripts activation may be crucial for QDR, emphasizing the
500 dynamic role of transcriptional reprogramming as a major contributor to fungal resistance (Niks *et al.*,
501 2015; French *et al.*, 2016; D., Yang *et al.*, 2021).

502 Regulatory divergence across *A. thaliana* accessions was generally of low magnitude, questioning the
503 adaptive value of this diversity. By contrast to tightly regulated core genes, shell and accessory genes
504 identified in our work may exhibit a high level of transcriptional noise, possibly underlying a bet-
505 hedging strategy to improve immunity (Viney and Reece, 2013; Urban and Johnston, 2018). In such a
506 strategy, noise may lead to stochastic activation of diversified immune responses in cell subsets. This
507 local immune response may be sufficient to limit pathogen colonization or may propagate through cell
508 to cell communication. Over long evolutionary time, the plasticity of gene expression may also
509 facilitate the acquisition of precise temporal and spatial expression patterns underlying QDR (Groen *et*
510 *al.*, 2020; Jones and Vandepoele, 2020). The recent advent of single-cell RNA-sequencing (Tang *et al.*,
511 2023) will allow testing cell population immunity mechanisms that were not accessible to bulk RNA
512 analyses.

513

514 **How predictable is quantitative disease resistance?**

515 There was no detectable phylogenetic signal associated with global transcriptome patterns and
516 resistance phenotype in our 23 *A. thaliana* accession panel, indicating that the heritability of these
517 traits at the species level is complex. Previous analyses reported that transcriptome variation tends to
518 recapitulate evolutionary relationships accurately at the interspecies level but loses precision for
519 closely-related species (Ma *et al.*, 2018; Winkelmüller *et al.*, 2021; Wu *et al.*, 2022). This may be due
520 to transcriptional noise being prevalent in a subset of QDR genes, or to the independent evolution of
521 sequence and regulatory polymorphisms at QDR loci (Tirosh and Barkai, 2008; Harrison *et al.*, 2012;
522 Uebbing *et al.*, 2016). Contrasted contributions of regulatory divergence and sequence variation to the
523 evolution of quantitative plant immunity may indeed result in independence between these
524 polymorphisms at the species level. QDR phenotypes may therefore be difficult to predict from
525 sequence information alone (Gentzbittel *et al.*, 2019).
526 In a correlation analysis, we identified at least 500 genes by accession subset, the expression of which
527 was significantly associated with QDR phenotype. By training Machine Learning (ML) models on plant
528 transcriptomes, Sia *et al*. found that information on expression of 0.5% of genes could be sufficient to
529 predict classes of disease phenotypes across multiple pathosystems (Sia *et al.*, 2023). The ML analysis
530 of QDR transcriptomes also revealed that multiple independent gene sets could yield similarly good
531 predictions of the disease phenotype (Sia *et al.*, 2023). In agreement, clustering based on global
532 transcriptome response to *S. sclerotiorum* defined four accession subsets, each harboring contrasted
533 levels of resistance, indicating that several regulatory networks may lead to a similar phenotypic
534 response. Sets of genes with expression correlated with resistance differed across subsets suggesting
535 that coordinated evolution of gene expression at the sub-species level could contribute to phenotypic
536 adaptation (Mezey *et al.*, 2008). This is in line with the analysis of the transcriptome of *Brassica rapa*
537 populations over multiple generations, which further showed rapid evolution through regulatory
538 divergence (Hamann *et al.*, 2021).
539 A corollary of this finding is that globally similar transcriptomes can produce very contrasted disease
540 phenotypes. This may be explained by a prevalent role of regulation at the post-transcriptional level in
541 QDR, although the massive transcriptional reprogramming induced by *S. sclerotiorum* inoculation
542 argues against this hypothesis. Alternatively, the QDR response network may be redundant or
543 structured to canalize similar downstream responses in spite of variable inputs (different pathogen
544 genotypes, environmental conditions, or plant genetic background) (Zhang *et al.*, 2017). This would be
545 consistent with QDR genes from the more recent gene age class showing higher protein-protein
546 connectivity than other genes from the same age class. Considering that lineage-specific genes often
547 participate in adaptation to biotic and abiotic stress (Tian *et al.*, 2012), genes from the most recent age

548 class may contribute to QDR plasticity. The existence of multiple resistance-associated transcriptomes
549 at the species level also suggests that even minor transcriptional variations in key regulators may play
550 a significant role in phenotypic modulation (Jenull *et al.*, 2021). Genes with co-varying expression
551 patterns, such as the top 500 co-expressed genes by accession subset, exhibit strong plasticity and may
552 influence the activity of core DEGs (Xing *et al.*, 2018). A limited set of core genes may have a substantial
553 direct impact on QDR and could each be influenced by numerous minor effect genes due to their
554 interactions within the broader gene networks (Liu *et al.*, 2019). Exploring regulatory mechanisms and
555 functions of lineage-specific genes presents an opportunity to identify new contributors to QDR.
556
557 **How does the regulation of fungal-responsive genes evolve?**
558
559 Our findings support the central role of core up-regulated DEGs in response to *Sclerotinia*, mediating
560 broad and durable resistance to fungal pathogens. Our analyses suggest that stable transcriptional
561 patterns of core genes were acquired, at least in part, by combining WRKY motifs in their 5'-regulatory
562 regions and high network connectivity. The emergence of cis-regulatory variants is recognized as the
563 primary source driving the acquisition of novel gene expression patterns. Variation in transcriptome
564 may be facilitated by regulatory elements or epigenetic mechanisms that alter gene expression even
565 before genetic variants arise in the population (Alvarez *et al.*, 2015). Our analyses point towards the
566 acquisition of WRKY binding motifs, known for their involvement in transcriptional regulation (Wani *et*
567 *al.*, 2021) as a potential mechanism for the stabilization of core gene expression at the species level.
568 When comparing the promoter sequences of QDR-associated genes within accession subsets, we
569 identified DAP motifs whose presence correlated with gene expression patterns, such as the
570 waycTTATCCAwwww DNA motif recognized by the MYB-related transcription factor AT5G56840. The
571 acquisition of this motif was associated with transcriptome modulation in our dataset, consistent with
572 the role of MYB transcription factors in regulating plant fungal immunity (Zhu *et al.*, 2021; Yu *et al.*,
573 2023). Given the unique DAP motifs enriched specifically in QDR responsive genes of each accession
574 subset, we propose that the gain or loss of DNA TF-binding motifs contributes significantly to
575 transcriptional variation at the species level. Contrary to our expectations, we did not find transposable
576 element families significantly associated with QDR transcriptome modulation at the species level.

577 Cis-regulatory variations arise from the emergence of novel enhancer sequences (Long *et al.*, 2016) or
578 from genome rearrangements that recruit new genes to transcriptionally active regions. Cis-regulatory
579 variations may also serve as a source for generating allele-specific transcripts involved in QDR (Fukuoka
580 *et al.*, 2014; P., Yang *et al.*, 2021). Novel enhancer activities often result from the co-option of
581 transcription factor binding sites already present in ancestral enhancers (Wittkopp and Kalay, 2012;
582 Macquet *et al.*, 2022). The acquisition of cis-regulatory enhancers in promoter regions is known to

583 drive the evolution of gene expression, shaping transcriptome patterns related to plant resistance
584 (Ogasahara *et al.*, 2022). The divergence of cis-regulatory motifs is suggested to be a key contributor
585 to the rapid transcriptional reprogramming essential for the broad-spectrum efficiency of plant
586 immune responses (Mine *et al.*, 2018). Most intraspecific variations can be attributed to tightly
587 constrained cis-associated differences influenced by linkage disequilibrium (Signor and Nuzhdin, 2018).
588 Consequently, variation in cis-regulatory elements across genotypes depends on various selective
589 forces, including abiotic and biotic environmental factors (Ricci *et al.*, 2019; Marand *et al.*, 2023). These
590 environmental constraints likely shaped the genome of accession subsets by acting on specific DAP
591 DNA motifs, facilitating the introduction of new genes or alleles involved in QDR.
592

593 **Acknowledgements**

594 We thank Sébastien Carrère and the LIPME bioinformatics platform for assistance with data storage
595 and manipulation including reads mapping. We are grateful to Adelin Barbacci for help in the
596 correlation regression analyses, to Marielle Barascud and Rémy Vincent for assistance in sample
597 collection for RNA sequencing, and to the QIP group at LIPME for discussions and suggestions. This
598 work was supported by the French Laboratory of Excellence project 'TULIP' (ANR-10-LABX-41; ANR-11-
599 IDEX-0002-02), l'Agence Nationale pour la Recherche (ANR-19-CE20-15, ANR-21-CE20-30), the
600 European Research Council (ERC-StG-336808), and the INRAE SPE division.

601

602 **Conflict of interest statement**

603 The authors declare that they have no competing interests to disclose.

604

605 **References:**

606 **Adachi, H., Contreras, M., Harant, A., *et al.*** (2019) An N-terminal motif in NLR immune receptors is
607 functionally conserved across distantly related plant species. *Elife*, **8**, 1–31.

608 **Aerts, N., Pereira Mendes, M. and Wees, S.C.M. Van** (2021) Multiple levels of crosstalk in hormone
609 networks regulating plant defense. *Plant J.*, **105**, 489–504.

610 **Alvarez, M., Schrey, A.W. and Richards, C.L.** (2015) Ten years of transcriptomics in wild populations:
611 What have we learned about their ecology and evolution? *Mol. Ecol.*, **24**, 710–725.

612 **Ando, T., Matsuda, T., Goto, K., *et al.*** (2018) Repeated inversions within a pannier intron drive
613 diversification of intraspecific colour patterns of ladybird beetles. *Nat. Commun.*, **9**, 1–13.

614 **Badet, T., Léger, O., Barascud, M., *et al*.** (2019) Expression polymorphism at the ARPC4 locus links the
615 actin cytoskeleton with quantitative disease resistance to *Sclerotinia sclerotiorum* in *Arabidopsis*
616 *thaliana*. *New Phytol.*, **222**, 480–496.

617 **Badet, T., Voisin, D., Mbengue, M., Barascud, M., Sucher, J., Sadon, P., Balagué, C., Roby, D. and**

618 **Raffaele, S.** (2017) Parallel evolution of the POQR prolyl oligo peptidase gene conferring plant
619 quantitative disease resistance. *PLoS Genet.*, **13**, 1–24.

620 **Bailey, T.L., Johnson, J., Grant, C.E. and Noble, W.S.** (2015) The MEME Suite. *Nucleic Acids Res.*, **43**,
621 W39–W49.

622 **Barbacci, A., Navaud, O., Mbengue, M., Barascud, M., Godiard, L., Khafif, M., Lacaze, A. and Raffaele,**
623 **S.** (2020) Rapid identification of an Arabidopsis NLR gene as a candidate conferring susceptibility
624 to *Sclerotinia sclerotiorum* using time-resolved automated phenotyping. *Plant J.*, **103**, 903–917.

625 **Barco, B., Kim, Y. and Clay, N.K.** (2019) Expansion of a core regulon by transposable elements
626 promotes Arabidopsis chemical diversity and pathogen defense. *Nat. Commun.*, **10**, 1–12.

627 **Berre, J.Y. Le, Gourgues, M., Samans, B., Keller, H., Panabières, F. and Attard, A.** (2017) Transcriptome
628 dynamic of Arabidopsis roots infected with *Phytophthora parasitica* identifies VQ29, a gene
629 induced during the penetration and involved in the restriction of infection. *PLoS One*, **12**, 1–25.

630 **Bolton, M.D., Thomma, B.P.H.J. and Nelson, B.D.** (2006) *Sclerotinia sclerotiorum* (Lib.) de Bary: Biology
631 and molecular traits of a cosmopolitan pathogen. *Mol. Plant Pathol.*, **7**, 1–16.

632 **Boyle, E.A., Li, Y.I. and Pritchard, J.K.** (2017) An Expanded View of Complex Traits: From Polygenic to
633 Omnigenic. *Cell*, **169**, 1177–1186.

634 **Brillada, C., Teh, O.K., Ditengou, F.A., *et al*.** (2021) Exocyst subunit Exo70B2 is linked to immune
635 signaling and autophagy. *Plant Cell*, **33**, 404–419.

636 **Coolen, S., Proietti, S., Hickman, R., *et al*.** (2016) Transcriptome dynamics of Arabidopsis during
637 sequential biotic and abiotic stresses. *Plant J.*, **86**, 249–267.

638 **Corwin, J.A. and Kliebenstein, D.J.** (2017) Quantitative Resistance: More Than Just Perception of a
639 Pathogen. *Plant Cell*, **29**, 655–665.

640 **Derbyshire, M., Denton-Giles, M., Hegedus, D., *et al*.** (2017) The complete genome sequence of the
641 phytopathogenic fungus *Sclerotinia sclerotiorum* reveals insights into the genome architecture of
642 broad host range pathogens. *Genome Biol. Evol.*, **9**, 593–618.

643 **Derbyshire, M.C. and Denton-Giles, M.** (2016) The control of sclerotinia stem rot on oilseed rape
644 (*Brassica napus*): current practices and future opportunities. *Plant Pathol.*, **65**, 859–877.

645 **Desclos-Theveniau, M., Arnaud, D., Huang, T.Y., Lin, G.J.C., Chen, W.Y., Lin, Y.C. and Zimmerli, L.**
646 (2012) The Arabidopsis lectin receptor kinase LecRK-V.5 represses stomatal immunity induced by
647 *Pseudomonas syringae* pv. *tomato* DC3000. *PLoS Pathog.*, **8**.

648 **Dodds, P.N. and Rathjen, J.P.** (2010) Plant immunity: Towards an integrated view of plant-pathogen
649 interactions. *Nat. Rev. Genet.*, **11**, 539–548.

650 **Eckardt, N.A.** (2011) BIK1 function in plant growth and defense signaling. *Plant Cell*, **23**, 2806.

651 **Emms, D.M. and Kelly, S.** (2019) OrthoFinder: Phylogenetic orthology inference for comparative
652 genomics. *Genome Biol.*, **20**, 1–14.

653 **Filichkin, S.A., Breton, G., Priest, H.D., *et al*.** (2011) Global profiling of rice and poplar transcriptomes
654 highlights key conserved Circadian-controlled pathways and cis-regulatory modules. *PLoS One*, **6**.

655 **French, E., Kim, B.S. and Iyer-Pascuzzi, A.S.** (2016) Mechanisms of quantitative disease resistance in
656 plants. *Semin. Cell Dev. Biol.*, **56**, 201–208.

657 **Fukuoka, S., Yamamoto, S.-I., Mizobuchi, R., *et al*.** (2014) Multiple functional polymorphisms in a
658 single disease resistance gene in rice enhance durable resistance to blast. *Sci. Rep.*, **4**, 4550.

Gentzbittel, L., Ben, C., Mazurier, M., Shin, M.G., Lorenz, T., Rickauer, M., Marjoram, P., Nuzhdin, S. V. and Tatarinova, T. V. (2019) WhoGEM: An admixture-based prediction machine accurately predicts quantitative functional traits in plants. *Genome Biol.*, **20**, 1–20.

Goodstein, D.M., Shu, S., Howson, R., *et al*. (2012) Phytozome: A comparative platform for green plant genomics. *Nucleic Acids Res.*, **40**, 1178–1186.

Gou, M., Balint-Kurti, P., Xu, M. and Yang, Q. (2023) Quantitative disease resistance: Multifaceted players in plant defense. *J. Integr. Plant Biol.*, **65**, 594–610.

Groen, S.C., Ćalić, I., Joly-Lopez, Z., *et al.* (2020) The strength and pattern of natural selection on gene expression in rice. *Nature*, **578**, 572–576.

Guindon, S., Dufayard, J.F., Lefort, V., Anisimova, M., Hordijk, W. and Gascuel, O. (2010) New algorithms and methods to estimate maximum-likelihood phylogenies: Assessing the performance of PhyML 3.0. *Syst. Biol.*, **59**, 307–321.

Guo, L., Yu, H., Wang, B., *et al.* (2021) Metatranscriptomic comparison of endophytic and pathogenic fusarium-arabidopsis interactions reveals plant transcriptional plasticity. *Mol. Plant-Microbe Interact.*, **34**, 1071–1083.

Hamann, E., Pauli, C.S., Joly-Lopez, Z., Groen, S.C., Rest, J.S., Kane, N.C., Purugganan, M.D. and Franks, S.J. (2021) Rapid evolutionary changes in gene expression in response to climate fluctuations. *Mol. Ecol.*, **30**, 193–206.

Han, X. and Tsuda, K. (2022) Evolutionary footprint of plant immunity. *Curr. Opin. Plant Biol.*, **67**, 102209.

Harrison, P.W., Wright, A.E. and Mank, J.E. (2012) The evolution of gene expression and the transcriptome-phenotype relationship. *Semin. Cell Dev. Biol.*, **23**, 222–229.

Hillmer, R.A., Tsuda, K., Rallapalli, G., *et al*. (2017) The highly buffered Arabidopsis immune signaling network conceals the functions of its components G. Coaker, ed. *PLoS Genet.*, **13**, e1006639.

Hoang, D.T., Chernomor, O., Haeseler, A. Von, Minh, B.Q. and Vinh, L.S. (2018) UFBoot2: Improving the ultrafast bootstrap approximation. *Mol. Biol. Evol.*, **35**, 518–522.

Iakovidis, M., Chung, E.H., Saile, S.C., Sauberzweig, E. and Kasmi, F. El (2022) The emerging frontier of plant immunity's core hubs. *FEBS J.*, **290**, 3311–3335.

Ito, H., Gaubert, H., Bucher, E., Mirouze, M., Vaillant, I. and Paszkowski, J. (2011) An siRNA pathway prevents transgenerational retrotransposition in plants subjected to stress. *Nature*, **472**, 115–120.

Jenull, S., Tscherner, M., Kashko, N., Shivarathri, R., Stoiber, A., Chauhan, M., Petryshyn, A., Chauhan, N. and Kuchler, K. (2021) Transcriptome Signatures Predict Phenotypic Variations of Candida auris. *Front. Cell. Infect. Microbiol.*, **11**, 1–13.

Jones, D.M. and Vandepoele, K. (2020) Identification and evolution of gene regulatory networks: insights from comparative studies in plants. *Curr. Opin. Plant Biol.*, **54**, 42–48.

Kalyaanamoorthy, S., Minh, B.Q., Wong, T.K.F., Haeseler, A. von and Jermiin, L.S. (2017) ModelFinder: fast model selection for accurate phylogenetic estimates. *Nat. Methods*, **14**, 587–589.

Kim, Y., Tsuda, K., Igarashi, D., Hillmer, R.A., Sakakibara, H., Myers, C.L. and Katagiri, F. (2014) Mechanisms underlying robustness and tunability in a plant immune signaling network. *Cell Host Microbe*, **15**, 84–94.

701 **Kou, Y. and Wang, S.** (2010) Broad-spectrum and durability: understanding of quantitative disease
702 resistance. *Curr. Opin. Plant Biol.*, **13**, 181–185.

703 **Kusch, S., Larrouy, J., Ibrahim, H.M.M., *et al.*** (2022) Transcriptional response to host chemical cues
704 underpins the expansion of host range in a fungal plant pathogen lineage. *ISME J.*, **16**, 138–148.

705 **Lasky, J.R., Marais, D.L. Des, Lowry, D.B., Povolotskaya, I., McKay, J.K., Richards, J.H., Keitt, T.H. and**
706 **Juenger, T.E.** (2014) Natural variation in abiotic stress responsive gene expression and local
707 adaptation to climate in *Arabidopsis thaliana*. *Mol. Biol. Evol.*, **31**, 2283–2296.

708 **Liu, X., Li, Y.I., Pritchard, J.K., Liu, X., Li, Y.I. and Pritchard, J.K.** (2019) Trans Effects on Gene Expression
709 Can Drive Omnigenic Inheritance Theory Trans Effects on Gene Expression Can Drive Omnigenic
710 Inheritance. *Cell*, **177**, 1022-1034.e6.

711 **Long, H.K., Prescott, S.L. and Wysocka, J.** (2016) Ever-Changing Landscapes: Transcriptional Enhancers
712 in Development and Evolution. *Cell*, **167**, 1170–1187.

713 **Love, M.I., Huber, W. and Anders, S.** (2014) Moderated estimation of fold change and dispersion for
714 RNA-seq data with DESeq2. *Genome Biol.*, **15**, 1–21.

715 **Ma, S., Avanesov, A.S., Porter, E., Lee, B.C., Mariotti, M., Zemskaya, N., Guigo, R., Moskalev, A.A.**
716 **and Gladyshev, V.N.** (2018) Comparative transcriptomics across 14 Drosophila species reveals
717 signatures of longevity. *Aging Cell*, **17**, 1–15.

718 **Macquet, J., Mounichetty, S. and Raffaele, S.** (2022) Genetic co-option into plant–filamentous
719 pathogen interactions. *Trends Plant Sci.*, **27**, 1144–1158.

720 **Makarevitch, I., Waters, A.J., West, P.T., Stitzer, M., Hirsch, C.N., Ross-Ibarra, J. and Springer, N.M.**
721 (2015) Transposable Elements Contribute to Activation of Maize Genes in Response to Abiotic
722 Stress. *PLoS Genet.*, **11**.

723 **Marand, A.P., Eveland, A.L., Kaufmann, K. and Springer, N.M.** (2023) cis-Regulatory Elements in Plant
724 Development, Adaptation, and Evolution. *Annu. Rev. Plant Biol.*, **74**, 111–137.

725 **Mezey, J.G., Nuzhdin, S. V., Ye, F. and Jones, C.D.** (2008) Coordinated evolution of co-expressed gene
726 clusters in the Drosophila transcriptome. *BMC Evol. Biol.*, **8**, 1–17.

727 **Mine, A., Seyfferth, C., Kracher, B., Berens, M.L., Becker, D. and Tsuda, K.** (2018) The Defense
728 Phytohormone Signaling Network Enables Rapid, High-Amplitude Transcriptional
729 Reprogramming during Effector-Triggered Immunity. *Plant Cell*, **30**, 1199–1219.

730 **Monteiro, F. and Nishimura, M.T.** (2018) Structural, functional, and genomic diversity of plant NLR
731 proteins: An evolved resource for rational engineering of plant immunity. *Annu. Rev.*
732 *Phytopathol.*, **56**, 243–267.

733 **Moscou, M.J., Lauter, N., Steffenson, B. and Wise, R.P.** (2011) Quantitative and qualitative stem rust
734 resistance factors in barley are associated with transcriptional suppression of defense regulons.
735 *PLoS Genet.*, **7**, e1002208.

736 **Mwape, V.W., Mobegi, F.M., Regmi, R., Newman, T.E., Kamphuis, L.G. and Derbyshire, M.C.** (2021)
737 Analysis of differentially expressed *Sclerotinia sclerotiorum* genes during the interaction with
738 moderately resistant and highly susceptible chickpea lines. *BMC Genomics*, **22**, 1–14.

739 **Nakamura, T., Yamada, K.D., Tomii, K. and Katoh, K.** (2018) Parallelization of MAFFT for large-scale
740 multiple sequence alignments. *Bioinformatics*, **34**, 2490–2492.

741 **Nelson, R.M., Pettersson, M.E. and Carlborg, Ö.** (2013) A century after Fisher: Time for a new
742 paradigm in quantitative genetics. *Trends Genet.*, **29**, 669–676.

743 **Nguyen, L.T., Schmidt, H.A., Haeseler, A. Von and Minh, B.Q.** (2015) IQ-TREE: A fast and effective
744 stochastic algorithm for estimating maximum-likelihood phylogenies. *Mol. Biol. Evol.*, **32**, 268–
745 274.

746 **Niks, R.E., Qi, X. and Marcel, T.C.** (2015) Quantitative Resistance to Biotrophic Filamentous Plant
747 Pathogens: Concepts, Misconceptions, and Mechanisms. *Annu. Rev. Phytopathol.*, **53**, 445–470.

748 **O'Malley, R.C., Huang, S.S.C., Song, L., Lewsey, M.G., Bartlett, A., Nery, J.R., Galli, M., Gallavotti, A.**
749 **and Ecker, J.R.** (2016) Cistrome and Epicistrome Features Shape the Regulatory DNA Landscape.
750 *Cell*, **165**, 1280–1292.

751 **Ogasahara, T., Kouzai, Y., Watanabe, M., et al.** (2022) Time-series transcriptome of Brachypodium
752 distachyon during bacterial flagellin-induced pattern-triggered immunity. *Front. Plant Sci.*, **13**, 1–
753 16.

754 **Oughtred, R., Rust, J., Chang, C., et al.** (2021) The BioGRID database: A comprehensive biomedical
755 resource of curated protein, genetic, and chemical interactions. *Protein Sci.*, **30**, 187–200.

756 **Pertea, G. and Pertea, M.** (2020) GFF Utilities: GffRead and GffCompare. *F1000Research*, **9**, 1–20.

757 **Peyraud, R., Mbengue, M., Barbacci, A. and Raffaele, S.** (2019) Intercellular cooperation in a fungal
758 plant pathogen facilitates host colonization. , **116**, 3193–3201.

759 **Pi, L., Zhang, Y., Wang, J., Wang, N., Yin, Z. and Dou, D.** (2023) A G-type lectin receptor-like kinase in
760 *Nicotiana benthamiana* enhances resistance to the fungal pathogen *Sclerotinia sclerotiorum* by
761 complexing with CERK1/LYK4. *Phytopathol. Res.*, **5**.

762 **Pink, H., Talbot, A., Carter, R., *et al*.** (2023) Identification of Lactuca sativa transcription factors
763 impacting resistance to *Botrytis cinerea* through predictive network inference. *bioRxiv*, **549542**.

764 **Pruitt, R.N., Locci, F., Wanke, F., *et al.*** (2021) The EDS1–PAD4–ADR1 node mediates Arabidopsis
765 pattern-triggered immunity. *Nature*, **598**, 495–499.

766 **Ricci, W.A., Lu, Z., Ji, L., et al.** (2019) Widespread long-range cis-regulatory elements in the maize
767 genome. *Nat. Plants*, **5**, 1237–1249.

768 **Robinson, M.D., McCarthy, D.J. and Smyth, G.K.** (2010) edgeR : a Bioconductor package for
769 differential expression analysis of digital gene expression data. *Bioinformatics*, **26**, 139–140.

770 **Roux, F., Voisin, D., Badet, T., Balagué, C., Barlet, X., Huard-Chauveau, C., Roby, D. and Raffaele, S.**
771 (2014) Resistance to phytopathogens e tutti quanti: Placing plant quantitative disease resistance
772 on the map. *Mol. Plant Pathol.*, **15**, 427–432.

773 **Rubiato, H.M., Liu, M., O'Connell, R.J. and Nielsen, M.E.** (2022) Plant SYP12 syntaxins mediate an
774 evolutionarily conserved general immunity to filamentous pathogens. *Elife*, **11**, 1–21.

775 **Shankar, R., Bhattacharjee, A. and Jain, M.** (2016) Transcriptome analysis in different rice cultivars
776 provides novel insights into desiccation and salinity stress responses. *Sci. Rep.*, **6**, 1–15.

777 **Shumate, A. and Salzberg, S.L.** (2021) Liftoff: Accurate mapping of gene annotations. *Bioinformatics*,
778 **37**, 1639–1643.

779 **Sia, J., Zhang, W., Cheng, M., Bogdan, P. and Cook, D.E.** (2023) Machine learning general
780 transcriptional predictors of plant disease. *bioRxiv*, **10.1101/20**.

781 **Signor, S.A. and Nuzhdin, S. V.** (2018) The Evolution of Gene Expression in cis and trans. *Trends Genet.*,
782 **34**, 532–544.

783 **Soltis, Nicole E., Caseys, C., Zhang, W., Corwin, J.A., Atwell, S. and Kliebenstein, D.J.** (2020) Pathogen

genetic control of transcriptome variation in the *Arabidopsis thaliana* - *Botrytis cinerea* pathosystem. *Genetics*, **215**, 253–266.

Soltis, Nicole E, Zhang, W., Corwin, J.A., Atwell, S. and Daniel, J. (2020) Pathogen genetic control of transcriptome variation in the. *Genetics*, **215**, 253–266.

Stotz, H.U., Sawada, Y., Shimada, Y., Hirai, M.Y., Sasaki, E., Krischke, M., Brown, P.D., Saito, K. and Kamiya, Y. (2011) Role of camalexin, indole glucosinolates, and side chain modification of glucosinolate-derived isothiocyanates in defense of Arabidopsis against *Sclerotinia sclerotiorum*. *Plant J.*, **67**, 81–93.

Studer, A., Zhao, Q., Ross-Ibarra, J. and Doebley, J. (2011) Identification of a functional transposon insertion in the maize domestication gene tb1. *Nat. Genet.*, **43**, 1160–1163.

Sucher, J., Mbengue, M., Dresen, A., Barascud, M., Didelon, M., Barbacci, A. and Raffaele, S. (2020) Phylotranscriptomics of the pentapetalae reveals frequent regulatory variation in plant local responses to the fungal pathogen *Sclerotinia sclerotiorum*. *Plant Cell*, **32**, 1820–1844.

Tang, B., Feng, L., Hulin, M.T., Ding, P. and Ma, W. (2023) Cell-type-specific responses to fungal infection in plants revealed by single-cell transcriptomics. *Cell Host Microbe*, **31**, 1732-1747.e5..

Tian, C.F., Zhou, Y.J., Zhang, Y.M., *et al.* (2012) Comparative genomics of rhizobia nodulating soybean suggests extensive recruitment of lineage-specific genes in adaptations. *Proc. Natl. Acad. Sci. U. S. A.*, **109**, 8629–8634.

Tirosh, I. and Barkai, N. (2008) Evolution of gene sequence and gene expression are not correlated in yeast. *Trends Genet.*, **24**, 109–113.

Tsuda, K. and Somssich, I.E. (2015) Transcriptional networks in plant immunity. *New Phytol.*, **206**, 932–947.

Uebbing, S., Künstner, A., Mäkinen, H., et al. (2016) Divergence in gene expression within and between two closely related flycatcher species. *Mol. Ecol.*, **25**, 2015–2028.

Urban, E.A. and Johnston, R.J. (2018) Buffering and Amplifying Transcriptional Noise During Cell Fate Specification. *Front. Genet.*, **9**, 1–14.

Viney, M. and Reece, S.E. (2013) Adaptive noise. *Proc. R. Soc. B Biol. Sci.*, **280**.

Wang, X., Werren, J.H. and Clark, A.G. (2016) Allele-Specific Transcriptome and Methylome Analysis Reveals Stable Inheritance and Cis-Regulation of DNA Methylation in Nasonia. *PLoS Biol.*, **14**, 1–21.

Wang, Z., Ma, L.Y., Cao, J., Li, Y.L., Ding, L.N., Zhu, K.M., Yang, Y.H. and Tan, X.L. (2019) Recent Advances in Mechanisms of Plant Defense to *Sclerotinia sclerotiorum*. *Front. Plant Sci.*, **10**, 1–14.

Wang, Z., Yang, L., Jander, G., Bhawal, R., Zhang, S., Liu, Z., Oakley, A. and Hua, J. (2022) AIG2A and AIG2B limit the activation of salicylic acid-regulated defenses by tryptophan-derived secondary metabolism in Arabidopsis. *Plant Cell*, **34**, 4641–4660.

Wani, S.H., Anand, S., Singh, B., Bohra, A. and Joshi, R. (2021) WRKY transcription factors and plant defense responses: latest discoveries and future prospects. *Plant Cell Rep.*, **40**, 1071–1085.

Westrick, N.M., Ranjan, A., Jain, S., Grau, C.R., Smith, D.L. and Kabbage, M. (2019) Gene regulation of *Sclerotinia sclerotiorum* during infection of Glycine max: On the road to pathogenesis. *BMC Genomics*, **20**, 1–22.

Winkelmüller, T.M., Entila, F., Anver, S., *et al*. (2021) Gene expression evolution in pattern-triggered immunity within *Arabidopsis thaliana* and across Brassicaceae species. *Plant Cell*, **33**, 1863–1887.

826 **Wittkopp, P.J. and Kalay, G.** (2012) Cis-regulatory elements: Molecular mechanisms and evolutionary
827 processes underlying divergence. *Nat. Rev. Genet.*, **13**, 59–69.

828 **Wu, J., Zhao, Q., Yang, Q., *et al.*** (2016) Comparative transcriptomic analysis uncovers the complex
829 genetic network for resistance to *Sclerotinia sclerotiorum* in *Brassica napus*. *Sci. Rep.*, **6**, 1–16.

830 **Wu, Q., Tong, W., Zhao, H., *et al.*** (2022) Comparative transcriptomic analysis unveils the deep
831 phylogeny and secondary metabolite evolution of 116 Camellia plants. *Plant J.*, **111**, 406–421.

832 **Xing, S., Tao, C., Song, Z., Liu, W., Yan, J., Kang, L., Lin, C. and Sang, T.** (2018) Coexpression network
833 revealing the plasticity and robustness of population transcriptome during the initial stage of
834 domesticating energy crop *Miscanthus lutarioriparius*. *Plant Mol. Biol.*, **97**, 489–506.

835 **Yang, D., Li, S., Xiao, Y., Lu, L., Zheng, Z., Tang, D. and Cui, H.** (2021) Transcriptome analysis of rice
836 response to blast fungus identified core genes involved in immunity. *Plant Cell Environ.*, **44**, 3103–
837 3121.

838 **Yang, P., Scheuermann, D., Kessel, B., *et al.*** (2021) Alleles of a wall-associated kinase gene account for
839 three of the major northern corn leaf blight resistance loci in maize. *Plant J.*, **106**, 526–535.

840 **Yu, C.P., Chen, S.C.C., Chang, Y.M., *et al.*** (2015) Transcriptome dynamics of developing maize leaves
841 and genomewide prediction of cis elements and their cognate transcription factors. *Proc. Natl.*
842 *Acad. Sci. U. S. A.*, **112**, E2477–E2486.

843 **Yu, Yongbo, Zhang, S., Yu, Yang, Cui, N., Yu, G., Zhao, H., Meng, X. and Fan, H.** (2023) The pivotal role
844 of MYB transcription factors in plant disease resistance. *Planta*, **258**, 1–10.

845 **Zhang, J., Li, Y., Bao, Q., Wang, H. and Hou, S.** (2022) Plant elicitor peptide 1 fortifies root cell walls
846 and triggers a systemic root-to-shoot immune signaling in Arabidopsis. *Plant Signal. Behav.*, **17**.

847 **Zhang, W., Corwin, J.A., Copeland, D., *et al.*** (2017) Plastic Transcriptomes Stabilize Immunity to
848 Pathogen Diversity: The Jasmonic Acid and Salicylic Acid Networks within the Arabidopsis/
849 Botrytis Pathosystem. *Plant Cell*, **29**, 2727–2752.

850 **Zhang, W., Corwin, J.A., Copeland, D.H., Feusier, J., Eshbaugh, R., Cook, D.E., Atwell, S. and**
851 **Kliebenstein, D.J.** (2019) Plant–necrotroph co-transcriptome networks illuminate a metabolic
852 battlefield. *Elife*, **8**, 1–32.

853 **Zhang, W., Fraiture, M., Kolb, D., *et al.*** (2013) Arabidopsis RECEPTOR-LIKE PROTEIN30 and receptor-
854 like kinase SUPPRESSOR OF BIR1-1/EVERSHED mediate innate immunity to necrotrophic fungi.
855 *Plant Cell*, **25**, 4227–4241.

856 **Zhou, J., Sun, A. and Xing, D.** (2013) Modulation of cellular redox status by thiamine-activated NADPH
857 oxidase confers Arabidopsis resistance to Sclerotinia sclerotiorum. *J. Exp. Bot.*, **64**, 3261–3272.

858 **Zhu, Q.H., Stephen, S., Kazan, K., Jin, G., Fan, L., Taylor, J., Dennis, E.S., Helliwell, C.A. and Wang,**
859 **M.B.** (2013) Characterization of the defense transcriptome responsive to *Fusarium oxysporum*-
860 infection in Arabidopsis using RNA-seq. *Gene*, **512**, 259–266.

861 **Zhu, X., Li, X., He, Q., Guo, D., Liu, C., Cao, J., Wu, Z., Kang, Z. and Wang, X.** (2021) TaMYB29: A Novel
862 R2R3-MYB Transcription Factor Involved in Wheat Defense Against Stripe Rust. *Front. Plant Sci.*,
863 **12**.

864 **Zhu, Y., Duan, L., Zhu, C., Wang, L., He, Z., Yang, M. and Zhou, E.** (2023) Dual Transcriptome Analysis
865 Reveals That ChATG8 Is Required for Fungal Development, Melanization and Pathogenicity during
866 the Interaction between *Colletotrichum higginsianum* and *Arabidopsis thaliana*. *Int. J. Mol. Sci.*,
867 **24**.

Supplementary data

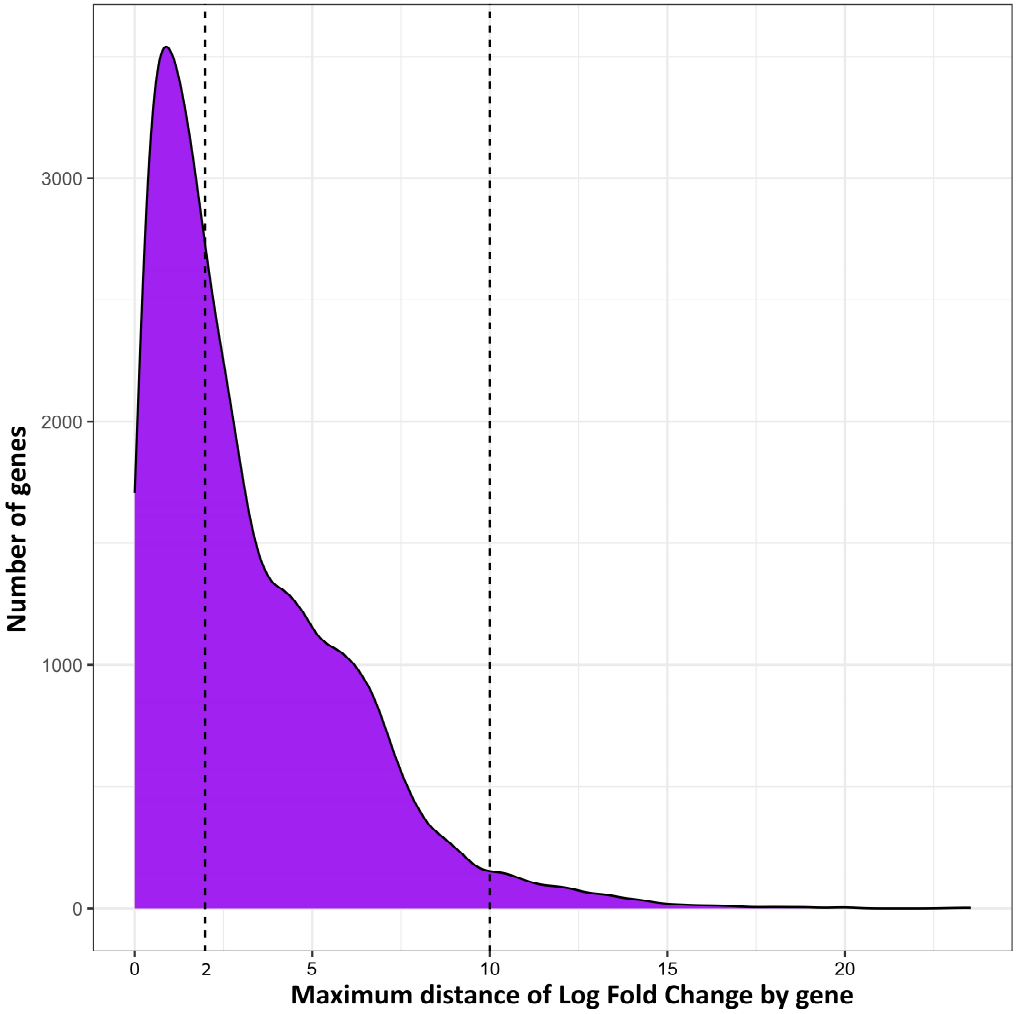

Supplemental Figures 1: Maximum distance of Log Fold Change by gene.

Density plot illustrating the maximum distance of Log Fold Change for each genes. The vertical dashed line indicates a maximum distance of 2 and 10 Log Fold Change.

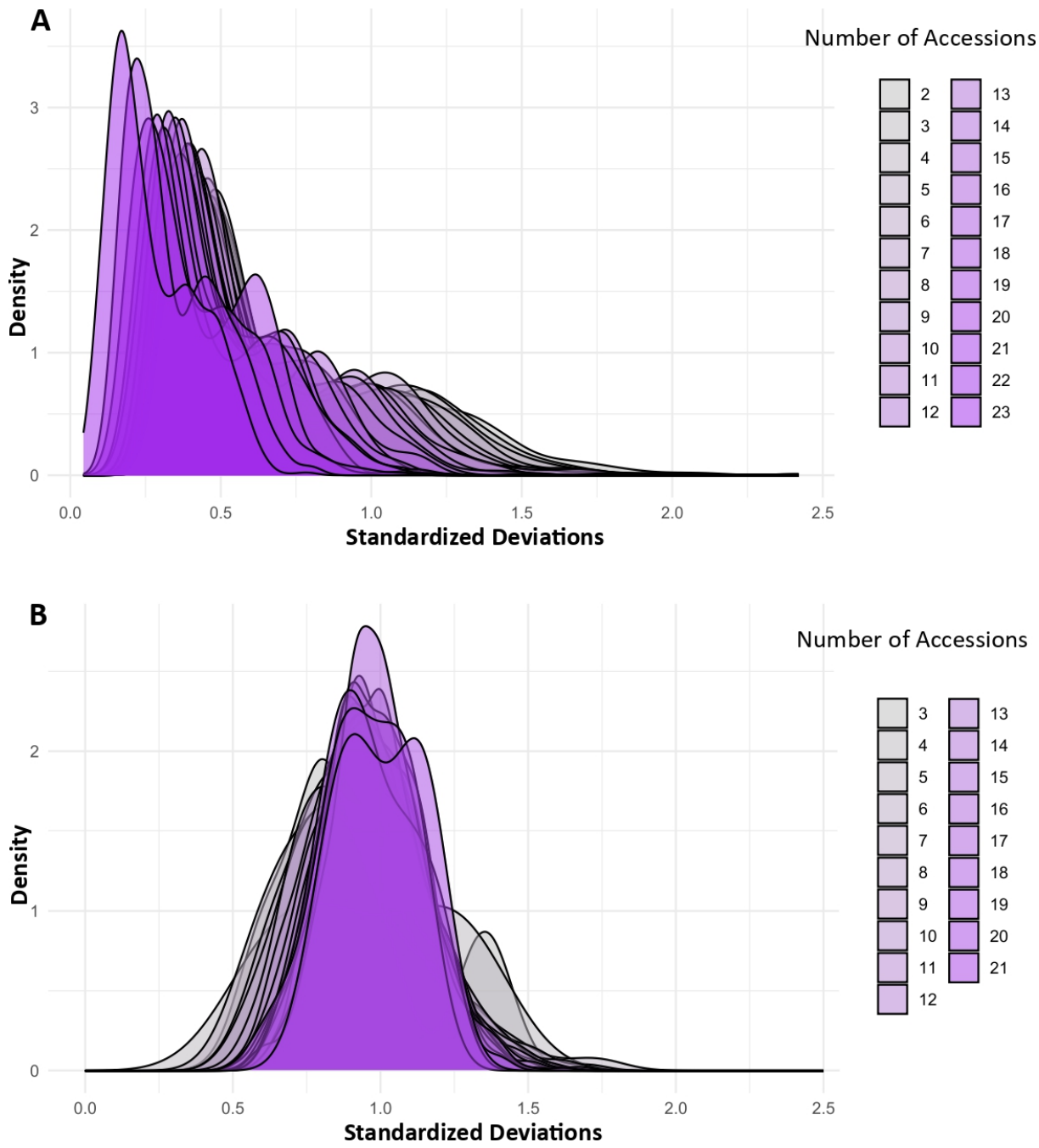

Supplemental Figures 2 : Log fold change for genes misregulated in 23 accessions exhibits higher stability compared to genes misregulated in fewer accessions.

A. Density plot illustrating the standard deviation of log fold change for genes misregulated in 2 to 23 accessions. **B.** Density plot generated from a randomized table. Genetic data was randomized by randomly shuffling the log fold change values within each accession. The number of accessions showing misregulation was estimated for each gene, along with the corresponding log fold change standard deviation.

885

886

887

888

889

890

891

892

893

894

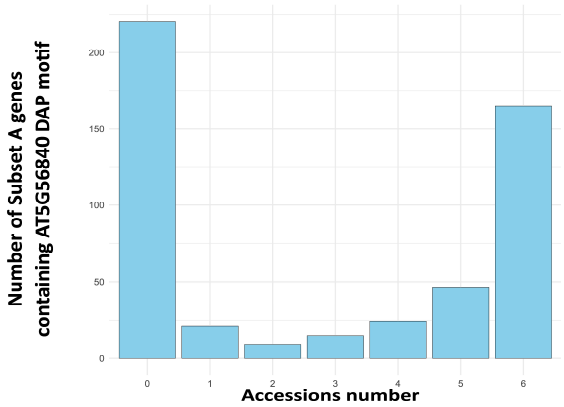

895 **Supplemental Figures 3: Variability in the presence of AT5G56840 DAP motif in promoters of**
896 **top500^{A} across the accessions subset A.**

897 The graph illustrates number of top500^{A} genes containing the AT5G56840 DAP motif across the
898 number of accessions for subset A, including Ang-0, Co-1, Se-0, Van-0, Kyoto and Ws-0. Mt-0 promoter
899 sequences were not available.